ATP 1778
pp: 1-18 (col.fig.: Nil)
PROD. TYPE: COM
ED: SNR
PAGN: Thanuja – SCAN: Lakshmi

ARTICLE IN PRESS

ELSEVIER

Journal of Atmospheric and Solar-Terrestrial Physics ▮▮▮ (▮▮▮▮) ▮▮▮–▮▮▮

Journal of ATMOSPHERIC AND SOLAR-TERRESTRIAL PHYSICS

www.elsevier.com/locate/jastp

Traveling wave packets of total electron content disturbances as deduced from global GPS network data

E.L. Afraimovich*, N.P. Perevalova, S.V. Voyeikov

Institute of Solar-Terrestrial Physics SD, Russian Academy of Sciences, P.O. Box 4026, Irkutsk 664033, Russia

Received 25 November 2002; received in revised form 10 July 2003; accepted 20 August 2003

Abstract

We identified a specific class of mid-latitude medium-scale traveling ionospheric disturbances (MSTIDs), namely traveling wave packets (TWPs) of total electron content (TEC) disturbances. For the first time, we present the TWP morphology for 105 days 1998–2001. A total number of the TEC series, with a duration of each series of about 2.3 h, exceeded 700,000. The data were obtained using the technology GLOBDET of global detection of ionospheric disturbances using a global network of GPS receivers, and the technique of GPS interferometry of TIDs, developed at the ISTP SD RAS. It was found that TWPs are observed no more than in 0.1–0.4% of all TEC series, most commonly during the daytime in winter and autumn. TWPs are quasi-periodic oscillations of TEC with a period of around 10–20 min, and a time duration of the order of 1 h. The TWP amplitudes exceed the amplitudes of "background" TEC fluctuations by one order of magnitude, as a minimum. The radius of spatial correlation of TWPs does not exceed 500–600 km (3–5 wavelengths). We carried out a detailed analysis of the spatial–temporal properties of TWPs by considering an example of the most conspicuous manifestation of TWPs on October 18, 2001 over California, USA. The velocity and direction of TWP displacement correspond to those of mid-latitude MSTIDs.

Keywords: Atmospheric acoustic-gravity waves; Medium-scale traveling ionospheric disturbances; Traveling wave packets; GPS; Total electron content

1. Introduction

The unremitting interest in investigations of atmospheric acoustic-gravity waves (AGW) over more than four decades dating back to Hines pioneering work (Hines, 1960; Hines and Reddy, 1967) is dictated by the important role played by these waves in the dynamics of the Earth's atmosphere. These research efforts have been addressed in a large number of publications, including a series of thorough reviews (Hocke and Schlegel, 1996; Oliver et al., 1997).

AGW typically show up in the ionosphere in the form of traveling ionospheric disturbances (TIDs) and are detected by various radio techniques. TIDs are classified as large-scale and medium-scale disturbances (LSTIDs and MSTIDs). LSTIDs have horizontal phase speeds between 400 and 1000 m/s (comparable with the sound velocity in the thermosphere), horizontal wavelengths greater than 1000 km and periods in the range of 30 min to 3 h. MSTIDs have horizontal phase velocities between 100 and 250 m/s (less than the sound velocity in the lower atmosphere), wavelengths of several hundred kilometers and periods between 15 and 60 min (Hocke and Schlegel, 1996). MSTIDs are observed predominantly during the daytime hours and are associated with AGW which are possibly generated in the lower atmosphere. LSTIDs are predominant in the night-time hours and are closely associated with geomagnetic and auroral activity.

It is known that the sources of medium-scale AGW can include natural processes of a different origin: magnetic storms, auroral phenomena, dynamical processes in the lower and middle atmosphere (e.g., convection, orography, shear flow, jet stream), the solar terminator, strong

* Corresponding author. Fax: +7-3952-462557.
E-mail address: afra@iszf.irk.ru (E.L. Afraimovich).

1364-6826/$ - see front matter © 2003 Published by Elsevier Ltd.
doi:10.1016/j.jastp.2003.08.007

earthquakes, volcanic eruptions, as well as anthropogenic influences (rocket launchings, explosions, nuclear tests). As a consequence the observed picture of the electron density disturbances is essentially a net interference wave field of AGWs of different origins and their interactions with the ionospheric plasma. Identifying of the AGW of a definite type from this field is a highly involved and generally an almost intractable problem.

The most reliable measurements of the main parameters of medium-scale AGW (parameters of the wave vector of the AGW, spectral and dispersion characteristics, etc.) can therefore be made only for a very rare, unusual type of MSTIDs, i.e. quasi-periodic (monochromatic) oscillations which are sometimes recorded as corresponding variations of the frequency Doppler shift F_D of the ionosphere-reflected HF radio signal (Davies and Jones, 1971; Waldock and Jones, 1987; Jacobson and Carlos, 1991; Yakovets et al., 1999).

Experiments of this kind were instrumental in investigating the spatial–temporal characteristics of MSTIDs in the form of a wave process, because such recordings are easy to identify visually with monochromatic individual AGW. Unfortunately, this was possible to accomplish for a very limited body of experimental data. Thus, Jacobson and Carlos (1991) managed to identify only a few monochromatic TIDs from their data obtained for more than 100 h of observation.

Yakovets et al. (1999) also recorded only a few realizations of monochromatic TIDs for two observing periods from the winter months of 1989 and 1990. Yakovets et al. (1999) used the term “wave packets” to designate the quasi-monochromatic variations of F_D, and they made an attempt to explain their origin on the basis of studying the phase structure of the oscillations. The authors of the cited reference observed two types of F_D-variations: quasi-stochastic TIDs, and monochromatic TIDs in the form of wave packets. They arrived at the conclusion that quasi-stochastic TIDs are characterized by a random phase behavior, a short length of coherence, and by a large vertical phase velocity. Wave packets show quasi-monochromatic oscillations of F_D, a larger length of coherence, and a smaller vertical phase velocity.

The term wave packets was first applied to ionospheric disturbances by Hines (1960). Following Hines (1960), we chose to utilize the term wave packets by expanding it to the term “traveling wave packets” (TWPs). The investigation made in this paper has brought out clearly that this designation describes most adequately the phenomenon involved.

Some authors associate the variations of the frequency Doppler shift F_D with MSTIDs that are generated during the passage of atmospheric fronts, tornadoes, and hurricanes (Baker and Davies, 1969; Bertin et al., 1975, 1978; Hung et al., 1978; Kersly and Rees, 1982; Stobie et al., 1983; Huang et al., 1985). It is only in some cases that these experiments observed quasi-monochromatic variations of F_D with periods of about 10 min (Huang et al., 1985).

Thus, in spite of the many years of experimental and theoretical studies, so far there is no clear understanding not only of the physical origin of the quasi-monochromatic MSTIDs but even of their morphology as well (the occurrence frequency as a function of geographical location, time, level of geomagnetic and meteorological activity, etc.).

To address these issues requires obtaining statistically significant sets of experimental data with good spatial resolution in order to study not only the morphological but also dynamic characteristics of quasi-monochromatic MSTIDs (the direction of their displacement, their propagation velocity, and the location of the possible disturbance source). Another important requirement implies the continuous, global character of observations, because such phenomena are temporally highly rare and spatially random.

Such a possibility is, for the first time, afforded by the use of the international ground-based network of two-frequency receivers of the navigation GPS system which at the beginning of 2002 consisted of no less than 1000 sites, with its data posted on the Internet, which opens up a new era of a global, continuous and fully computerized monitoring of ionospheric disturbances of a different class.

Regional dedicated GPS receivers have been deployed to date to solve a variety of problems in geodynamics, to investigate the ionosphere, and for other purposes. The most dense GEONET network consisting of 1000 receivers has been in operation in Japan for over 5 years now (Otsuka et al., 2002; Saito et al., 2001, 2002). This network provides an unprecedented (for transionospheric sounding systems) spatial resolution of about 1.15° thus opening up the new brand vistas for TEC mapping and measurement of space-time characteristics of TIDs (Saito et al., 2001, 2002; Shiokawa et al., 2002).

Analysis and identification of TWPs became possible through the use of the GLOBDET technology (developed at the ISTP) for global detection and determination of parameters of ionospheric disturbances of a different class (Afraimovich, 2000).

The objective of this paper is to study the morphology and spatial–temporal properties of TWPs using the data from the global network of GPS receivers. Section 2 provides general information about the experiment and gives a brief description of the method of TWP detecting. Section 3 presents our new evidence characterizing the TWP morphology. Section 4 is devoted to a detailed analysis of the spatial–temporal properties of TWPs by considering an example of the most pronounced manifestation of TWPs on October 18, 2001 as observed in California, USA. The discussion of our results compared with the findings reported by other authors is given in Section 5.

2. General information about the experiment and method of TWP detection

This paper presents, for the first time, the morphology of TWPs for 105 days of 1998–2001, with a different level of geomagnetic activity and with the number of stations of the global GPS network ranging from 10 to 300. The total number of the TEC series used in the analysis exceeds 700,000, corresponding to observations along a single receiver-satellite Line-of-Sight (LOS), with a duration of each series of about 2.3 h.

For a diversity of reasons, slightly differing sets of GPS stations were selected for different events to be analyzed; however, the geometry of experiment for all events was virtually identical. The stations coordinates are not given here for reasons of space. This information may be found at the electronic address http://lox.ucsd.edu/cgi-bin/allCoords.cgi? The global GPS covers rather densely North America and Europe, and to a much lesser extent Asia. GPS stations are more sparsely distributed on the Pacific and Atlantic Oceans. However, such coverage of the surface of the globe makes it possible, already today, to tackle the problem of global detection of disturbances with hither to unprecedented density of observations. Thus, in the Western hemisphere the corresponding number of stations can reach no less than 500 already today, and the number of LOS to the satellite can be no less than 2000–3000.

The area of California, USA, is particularly convenient for our investigations because of the large number of GPS stations (no less than 300) located over a relatively small area, which makes it possible to obtain a great variety of GPS arrays of a different configuration for a reliable determination of the dynamic TWP parameters using the method of GPS interferometry of TIDs (Afraimovich et al., 1998, 2000b).

For identifying the TEC pulsations of a possible meteorological origin, we processed an extensive data set from regional GPS networks in the area of California, the Caribbean basin, and South-East Asia, corresponding to the 17 strongest hurricanes and typhoons for the period 1998–2001 (http://www.solar.ifa.hawaii.edu/Tropical/).

The comparison of TWP characteristics with geomagnetic field variations was based on using the data from the INTERMAGNET network (INTERMAGNET, http://www.intermagnet.org/).

2.1. Method of processing the data from the global network: selection of TWPs

The standard GPS technology provides a means for wave disturbances detection based on phase measurements of slant TEC I_s (Hofmann-Wellenhof et al., 1992):

$$I_s = \frac{1}{40.308}\frac{f_1^2 f_2^2}{f_1^2 - f_2^2}[(L_1\lambda_1 - L_2\lambda_2) + const. + nL], \qquad (1)$$

where $L_1\lambda_1$ and $L_2\lambda_2$ are additional paths of the radio signal caused by the phase delay in the ionosphere, (m), L_1 and L_2 represent the number of phase rotations at the frequencies f_1 and f_2, λ_1 and λ_2 stand for the corresponding wavelengths (m), *const*. is the unknown initial phase path, caused by the unknown number of total phase rotations along the LOS, (m), and nL are errors in determining the phase path (m). TEC I_s is measured in m^{-2}, const 40.308 has the dimension (m^3/s^2).

Phase measurements in the GPS can be made with a high degree of accuracy corresponding to the error of TEC determination of at least $10^{14}\ m^{-2}$ when averaged on a 30-s time interval, with some uncertainty of the initial value of TEC, however (Hofmann-Wellenhof et al., 1992). This makes it possible to detect ionization irregularities and wave processes in the ionosphere over a wide range of amplitudes (up to 10^{-4} of the diurnal TEC variation) and periods (from 24 h to 5 min). The unit of TEC, which is equal to $10^{16}\ m^{-2}$ (*TECU*) and is commonly accepted in the literature, will be used in the following.

In some instances a convenient way for comparing TEC response characteristics from the GPS data with those obtained by analyzing the frequency Doppler shift in the HF range (Davies and Jones, 1971; Waldock and Jones, 1987; Jacobson and Carlos, 1991; Yakovets et al., 1999) is to estimate the frequency Doppler shift F_D from TEC series obtained by formula (1). To an approximation sufficient for the purpose of our investigation, a corresponding relationship was obtained by Davies (1969):

$$F_D = 13.5 \times 10^{-8} I_t'/f, \qquad (2)$$

where I_t' stands for the time derivative of TEC, F_D is measured in Hz, *const*. 13.5×10^{-8} has the dimension (m^2).

Primary data include series of slant values of TEC $I_s(t)$, as well as the corresponding series of elevations $\theta(t)_s$ and azimuths $\alpha(t)_s$ along LOS to the satellite calculated using our developed CONVTEC program which converts the GPS system standard RINEX-files on the INTERNET (Gurtner, 1993). For TWPs characteristics to be determined continuous series of $I_s(t)$ series of a duration of no less than 2.3 h are chosen.

Fig. 1 gives a schematic representation of the transionospheric sounding geometry. The axes z, y and x are directed, respectively, zenithward, northward N and eastward E. P—point of intersection of LOS to the satellite with a horizontal plane at the height h_{max} of the maximum of the ionospheric F_2-region (ionospheric piercing point of the GPS ray), S—subionospheric point (the point P projection on terrestrial surface), α_s—the azimuthal angle, counted off from the northward in a clockwise direction, and θ_s—the angle of elevation between the direction $\boldsymbol{r}$ along LOS to the satellite and the terrestrial surface at the reception site.

To normalize the response amplitude we converted the slant TEC to an equivalent "vertical" value (Klobuchar,

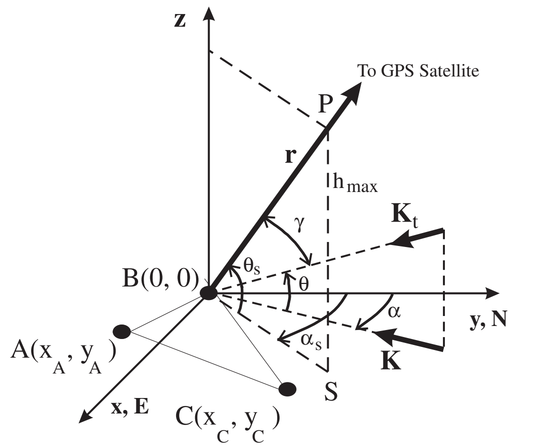

Fig. 1. Schematic representation of the transionospheric sounding geometry and geometry of the GPS-interferometer. The axes z, y and x are directed, respectively, zenithward, northward N and eastward E. P—point of intersection of LOS to the satellite with a horizontal plane at the height h_{max} of the maximum of the ionospheric F_2-region; S—subionospheric point; and α_s, θ_s—azimuth and elevation of the direction $\boldsymbol{r}$ along LOS to the satellite; α, θ—azimuth and elevation of the wave vector of TIDs $\boldsymbol{K}_t$; $\boldsymbol{K}$ is horizontal projection of $\boldsymbol{K}_t$; γ is the angle between the vectors $\boldsymbol{K}_t$ and $\boldsymbol{r}$. A, B, C—reception sites where dual-frequency multichannel GPS receivers are installed.

1986):

$$I = I_s \times \cos\left[\arcsin\left(\frac{R_z}{R_z + h_{max}}\cos\theta\right)\right], \tag{3}$$

where R_z is the Earth's radius.

The most reliable results from the determination of TWP parameters correspond to high values of elevations $\theta(t)_s$ of the LOS to the satellite because sphericity effects become reasonably small. All results in this study were obtained for elevations $\theta(t)_s$ larger than 30°.

The result of converting the slant TEC I_s to a vertical TEC by formula (3) depends weakly on the chosen value of h_{max} because of the large value of the ratio R_z/h_{max}. The scatter of the values of the coefficient of I_s in formula (3) for the least value of the elevation $\theta_s = 30°$ under consideration is ±0.018 in the case of a change of h_{max} by ±100 km from $h_{max} = 300$ km.

To eliminate variations of the regular ionosphere, as well as trends introduced by orbital motion of the satellite, we obtained TEC variations $dI(t)$ by filtering from the initial $I(t)$-series over the range of periods of 2–20 min.

The technology for global detection of TWPs that was developed at the ISTP SD RAS makes it possible to select—from a large amount of experimental material in the automatic mode—the TEC disturbances which can be assigned to a class of TWPs.

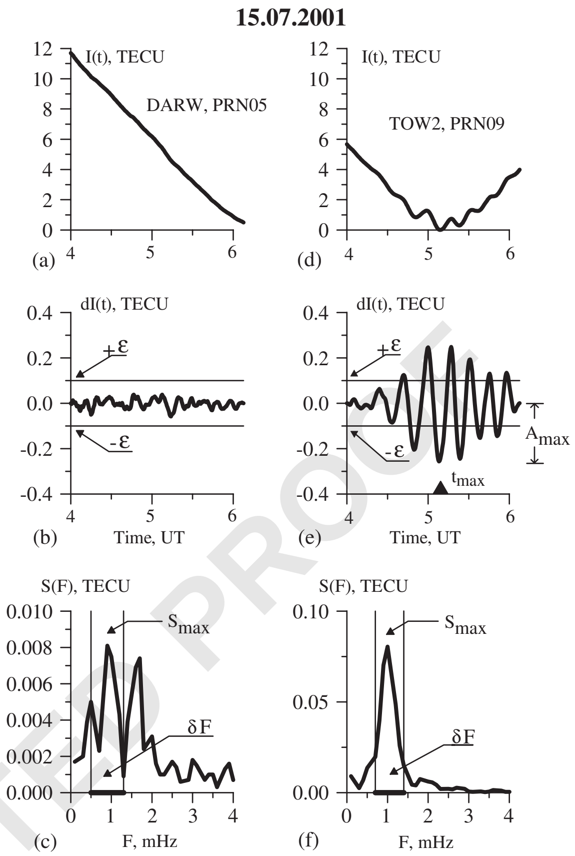

Fig. 2. An illustration of the selection of TWPs: (a) typical $I(t)$ series containing no TWP; (b) filtered $dI(t)$-series and (c) its spectrum $S(F)$. Panels (d,e,f) same but for the $I(t)$-series containing TWP. Shown in panels (a) and (d) are the station names and GPS satellite numbers. Levels of limitation in TWP amplitude ε are shown in panels (b) and (e) by horizontal lines. Boundaries of the range of frequencies δF used in the analysis are shown in panels (c) and (f) by vertical lines. Panel e shows the maximum value of the amplitude A_{max} and the time t_{max} corresponding to this amplitude. The arrows in panels (c) and (f) indicate the maximum values of the amplitude spectra S_{max}.

The selection of TEC series which could be ascribed to a class of TWPs was carried out by two criteria (Fig. 2). First of all, TEC variations were selected, for which the value of the rms exceeded a given threshold ε (in the present case $\varepsilon = 0.1$ *TECU*).

In addition, for each filtered series, we verified the fulfillment of the "quasi-monochromaticity" condition of TEC oscillations, for which the ratio R of a sum of spectral amplitude in the selected frequency band δF in the neighborhood of a maximum value of the amplitude S_{max}, to a sum of spectral amplitude outside the frequency band δF under consideration exceeded a given threshold R_{min} (in the present case $R_{min} = 2$).

Fig. 2 illustrates the selection process of the TWPs. Fig. 2a gives an example of weakly disturbed variations of the vertical TEC $I(t)$ as recorded on July 15, 2001 at station DARW (131.13°E; 12.8°S; satellite number PRN05). Fig. 2b presents the d$I(t)$-variations that were filtered from the initial $I(t)$-series. Thin horizontal lines show the specified threshold ε. The rms of the d$I(t)$-variations is 0.019 $TECU$, that is, does not reach the specified threshold $\varepsilon = 0.1$ $TECU$.

Fig. 2c illustrates the $S(F)$ spectrum of the series d$I(t)$ from Fig. 2b. Thin vertical lines show the boundaries of the frequency range δF. For this spectrum $R = 0.66$ is smaller than the specified $R_{\min} = 2$ and, hence, the series d$I(t)$ does not satisfy the condition of quasi-monochromaticity.

Figs. 2d–f plots the same dependencies as in Fig. 2a–c but for station TOW2 (147°E; 19.3°S; satellite number PRN09). It is evident from Fig. 2d that at the background of the slow TEC variations there are clearly identifiable (unusual for background TEC disturbances) oscillations in the form of a wave packet of a duration of about 1 h and with a typical period T in the range from 10 to 18 min. The oscillation amplitude of the detected wave packet exceeds one order of magnitude (as a minimum) the intensity of background TEC fluctuations of this range of periods (Afraimovich et al., 2001b).

The relative amplitude of such a response $\Delta I/I_0$ is considerable, 4%. As the background value of I_0 we used the absolute vertical TEC value of $I_0(t)$ for the site located at 19.3°S; 147°E, obtained from IONEX TEC maps. Global maps of the absolute global TEC value are calculated for each day of the year using the method described in (Mannucci et al., 1998), at four major research centers: Centre for Orbit Determination in Europe (CODE), Deutsches Zentrum fur Luft- und Raumfahrt e.V. (DLR), European Space Operations Center (ESOC), and University of New Brunswick (UNB). These maps may be accessed via the Internet (ftp://cddisa.gsfc.nasa.gov/pub/gps/products/ionex).

It is worthwhile to note that the two examples described above refer to the same time interval and to the stations spaced by a distance of no more than 1900 km from one another. This suggests a local character of the phenomenon and is in agreement with the overall sample statistics characterizing its spatial correlation (see Section 3).

The rms of the series d$I(t)$, shown in Fig. 2e, is 0.114 $TECU$, which is larger than the specified threshold $\varepsilon = 0.1$ $TECU$, and this series satisfies the condition for the rms. Fig. 2f presents the spectrum $S(F)$ of the series d$I(t)$, shown in Fig. 2e. For this spectrum $R = 3.71$, which is larger than the specified $R_{\min} = 2$, that is, in this case the series d$I(t)$ satisfies the condition of quasi-monochromaticity.

Fig. 2e shows the maximum value of the amplitude $A_{\max}$ of the packet and the time $t_{\max}$ corresponding to this amplitude.

When the filtered d$I(t)$-series satisfied the conditions described above, such an event was recognized as TWP.

Furthermore, for each such event, a special file stored information about the name, geographical latitude ϕ_s and longitude λ_s of the GPS station; the GPS satellite PRN number; the time $t_{\max}$ corresponding to the maximum value of the amplitude $A_{\max}$ of the TWP; the amplitude $A_{\max}$; the TWP oscillation period T; the R ratio; and about the value of the elevation $\theta_s(t)$ and the azimuth $\alpha_s(t)$ of the LOS to the satellite calculated for the time $t_{\max}$. The sample statistics, presented below, were obtained by processing such files for our selected value of $\varepsilon = 0.1$ $TECU$.

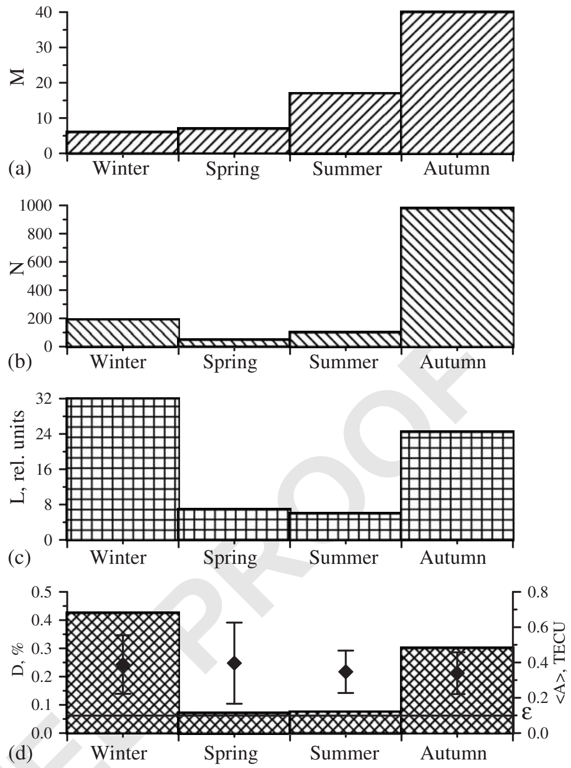

Fig. 3. Seasonal dependence of the density and maximum amplitude of TWPs: (a) number of days M of observation versus time of the year; (b) number of TWPs N; (c) mean number of TWPs per day $L = N/M$. (d) relative TWP density D obtained as the ratio of the number of TWPs N to the number of LOSs. Diamonds in panel (d) show the mean values, $\langle A \rangle$, of the maximum amplitudes $A_{\max}$ for each season, and vertical lines show their rms. The thick horizontal line shows the threshold in amplitude ($\varepsilon = 0.1$ $TECU$).

3. Morphology of TWPs

The method outlined above was used to obtain a series of TWPs totaling about 1300 cases, or about 0.2% of the total number of the TEC series considered (over 700,000). An analysis of the resulting statistics revealed a number of dependencies of the TWP parameters on different factors.

First of all, we consider the seasonal dependence of the occurrence rate and amplitude of the TWPs (Fig. 3). Fig. 3a plots the dependence of the number of days of observation

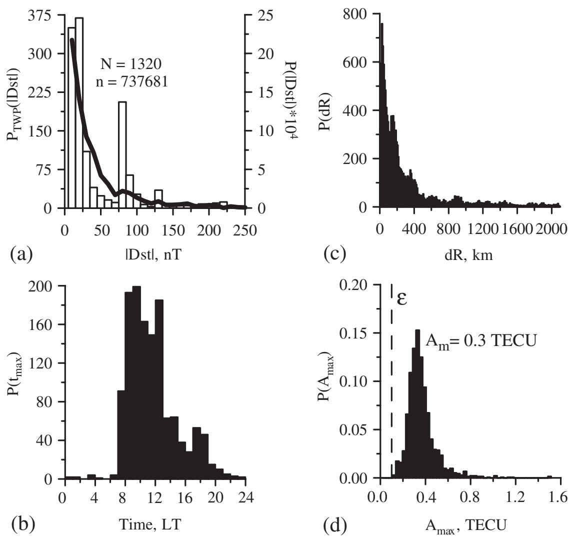

Fig. 4. Statistics of TWPs: (a) dependence $P_{TWP}(|Dst|)$ of the number of TWPs on the modulus of the Dst-index; the right scale on panel (a) shows distribution $P(|Dst|)$ for total number of TEC series; (b) diurnal distribution $P(t_{max})$ of the times t_{max} corresponding to the maximum amplitude A_{max} of the wave packet of the TEC disturbance; (c) histogram $P(dR)$ of the number of cases where TWPs within one 2.3-h time interval were observed at any two GPS stations, with the distance dR between them; (d) distribution $P(A_{max})$ of the maximum amplitude A_{max} of TWP. The vertical dashed line in panel (d) shows the threshold in amplitude $\varepsilon = 0.1$ $TECU$. Panel (a) shows the number N of the detected TWPs, and the total number n of TEC series. Panel (d) shows the most probable maximum amplitude A_m.

M on the time of the year. It is evident that statistically, the autumn season is represented best. Fig. 3b shows the seasonal dependence of the number of TWPs N. Fig. 3c plots the number of TWPs $L = N/M$ per day as a function of time of the year. This dependence has maxima in winter and in autumn.

The relative TWP density D, obtained as the ratio of the number of TWPs N to the number of receiver-satellite LOS, is presented in Fig. 3d. As is apparent from the figure, TWPs are observed in no more than 0.1–0.4% of the total number of TEC series, and much more frequently in winter (over 0.4%) and autumn (up to 0.3%) than in spring and summer (less than 0.1%).

Diamonds in Fig. 3d show the mean values, $\langle A \rangle$, of the maximum TWP amplitudes A_{max} for each season, and vertical lines show their rms. Thick horizontal line shows the threshold in amplitude $\varepsilon = 0.1$ $TECU$. The most probable value of $\langle A \rangle$ with a small scatter varies around the value 0.3 $TECU$, irrespective of the season.

Fig. 4d presents the normalized occurrence probability distribution of TWPs with the specified maximum amplitude of the packet A_{max}. The vertical dashed line shows the threshold in amplitude $\varepsilon = 0.1$ $TECU$. It was found that the most probable value of the amplitude A_m, also shown in Fig. 4d, is about 0.3 $TECU$. As was shown by Afraimovich et al. (2001b), the mean values of the TEC variation amplitude with the period of 20 min for the magnetically quiet and magnetically disturbed days do not exceed 0.01 $TECU$ and 0.07 $TECU$, respectively. Thus the most probable value of the amplitude A_m of TWPs exceeds the mean value of the TEC variation amplitude by one order of magnitude as a minimum for the magnetically quiet and 4–5 for the magnetically disturbed time intervals.

This estimate is consistent with the variation amplitude of the frequency Doppler shift F_D reported by Yakovets et al. (1999).

Fig. 4b presents the diurnal distribution $P(t_{max})$ of the times t_{max} corresponding to the maximum value of the amplitude A_{max} of the wave packet of TWPs. It is evident that most of the TWPs (about 87%) are observed during the daytime, from about 7:00 to 16:00 of local time, LT.

Fig. 4a plots the dependence $P_{TWP}(|Dst|)$ of the number of TWPs on the values of the geomagnetic activity index Dst taken by the modulus. In order to determine that there is some correlation between the number of observed TWPs and values of the $|Dst|$ index, one has to obtain the relative probability density of TWP occurrence for a given value of $|Dst|$. To do this requires dividing the number of TWP occurrence events for a given value of $|Dst|$ by the number of observations for a given value of $|Dst|$. The $P(|Dst|)$ distribution of the values of the $|Dst|$ index for all TEC series under consideration is shown by the thick line in Fig. 4a.

As is evident from Fig. 4a, the $P_{TWP}(|Dst|)$ distribution is almost identical to the $P(|Dst|)$ distribution, except for the outlier in the neighborhood of 80 nT. It is apparent from the $P(|Dst|)$ distribution that the number of observations in the neighborhood of 80 nT has also a peak, but this peak is less clearly pronounced than is the peak in the $P_{TWP}(|Dst|)$. The question arises as to whether this peak in the $P_{TWP}(|Dst|)$ is the manifestation of some correlation between the TWP occurrence and some values of the Dst-index in the neighborhood of 80 nT. In order to draw the conclusion about the existence of such a correlation, it is necessary that the increase of the number of TWP for values of Dst close to 80 nT is observed for a few days at least.

Indeed, we record not the exact time of TWP occurrence but the corresponding 2.3-h interval, and we use the hourly values of Dst assuming that TWPs were observed in the middle of the 2.3-h interval under consideration. In regions with a large number of GPS stations (in California, for example), TWPs could be observed for many LOSs for a single 2.3-h interval. We determined that the November 25, 2001 was responsible for the peak in the neighborhood of 80 nT in the $P_{TWP}(|Dst|)$ distribution. However, this unique event cannot serve as the basis for concluding that the TWP occurrence probability increases at values of $|Dst|$ close to 80 nT.

Thus, if we neglect the peak at 80 nT in the $P_{TWP}(|Dst|)$ when dividing $P_{TWP}(|Dst|)$ by $P(|Dst|)$, we obtain an almost uniform distribution of the relative density of the TWP occurrence probability depending on $|Dst|$-values. From this it follows that there is no significant correlation between the TWP occurrence probability and values of the geomagnetic disturbance index Dst.

The availability of a large number of GPS stations in some regions of the globe (in California, USA and West Europe, for example) makes it possible to determine not only the temporal but also spatial characteristics of TWPs. To estimate the radius of spatial correlation of events of this type we calculated the number of cases where the TWPs within a single 2.3-h time interval were observed at any two GPS stations separated by dR. Fig. 4c presents the histogram of values of $P(\mathrm{d}R)$ as a function of distance dR. It was found that the localization of the TWPs in space is strongly pronounced. In 82% of cases the distance dR does not exceed 500 km.

4. Traveling wave packets of total electron content disturbances as deduced from a case study of the October 18, 2001 event

Using the method of GPS interferometry of TIDs (Afraimovich et al., 1998, 2000b), we carried out a detailed analysis of the spatial–temporal properties of TWPs by considering an example of the most pronounced manifestation of TWPs on October 18, 2001 over California, USA. Numerous traveling ionospheric disturbances of the type of TWPs were recorded on that day between 15:00 and 18:00 UT using signals from several satellites, at many GPS stations located in California.

4.1. Geometry and general information about the October 18, 2001 experiment

The area of California within 220–260°E; 28–42°N is convenient for our investigations because of a large number of GPS stations located there, which makes it possible to obtain a great variety of GPS arrays of a different configuration for determining the TID parameters and provides a means of verifying the reliability of calculated data. It is also important that for the above-mentioned time interval 15:00–18:00 UT and for the chosen longitude range the local time varied from 08:00 to 11:00 LT, which reduces the level of background TEC fluctuations for the night-time.

Fig. 5 illustrates the geometry of the experiment of October 18, 2001. Crosses show the GPS stations, and dots show the position of subionospheric points for GPS receiver-satellite LOS. Since each receiver site observes simultaneously several (no less than four) GPS satellites, the number of TEC series far exceeds the number of stations, which enhances the capabilities of analysis. Fig. 5a presents the entire set of GPS stations used in the experiment. Figs. 5b and c show the stations and the subionospheric points where the TEC variations revealed TWPs with an amplitude exceeding the specified threshold $\varepsilon = 0.05$ $TECU$ (Fig. 5b) and $\varepsilon = 0.1$ $TECU$ (Fig. 5c). With the sole exception, TWPs were recorded along the LOSs over land, predominantly in the north-eastward direction. As is evident from Fig. 5, an increase of the recording threshold by a factor of two reduced the number of recorded events by a factor of two. Stations shown in Fig. 5c were used as the elements of the GPS arrays in calculating the TWP parameters.

The geomagnetic situation on October 18, 2001 may be characterized as a weakly disturbed one, which must lead to some increase of the level of background TEC

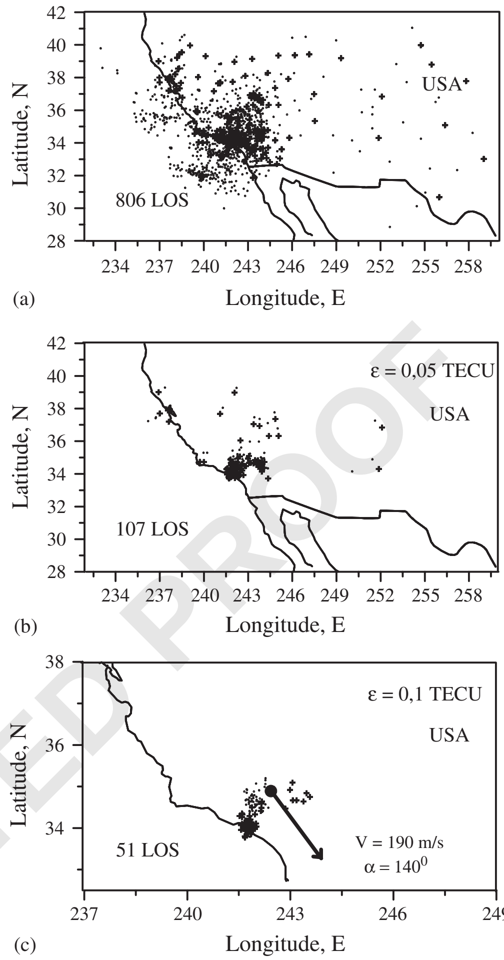

Fig. 5. Geometry of the experiment on detection of TWPs on October 18, 2001 in California, USA, from 15:00 to 18:00 UT. Crosses show the GPS stations, and dots show the location of subionospheric points for LOSs. Panel (a) presents the entire set of GPS stations used in the experiment. Panels (b) and (c) show the stations and subionospheric points where the TEC variations revealed TWPs with an amplitude exceeding the specified threshold ε: (b) $\varepsilon = 0.05$ $TECU$; (c) $\varepsilon = 0.1$ $TECU$. Numbers in all panels show the total number of LOSs shown in the panel. The vector $\boldsymbol{K}$ in panel (c) designate the direction and velocity of TWP.

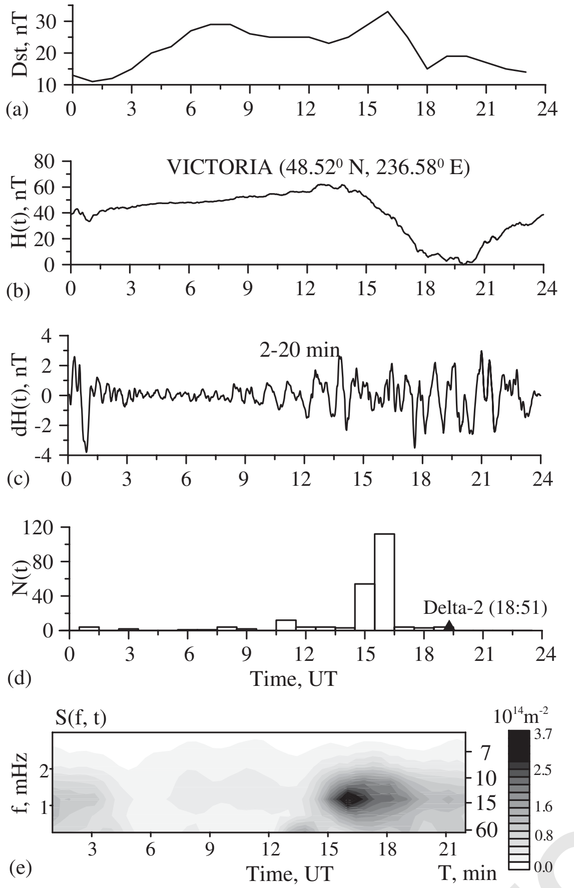

Fig. 6. Geomagnetic field *Dst*-variations (a) on October 18, 2001. $H(t)$-variations of the horizontal component of the geomagnetic field as recorded at station Victoria (236.58°E; 48.52°N) (b) $\mathrm{d}H(t)$-variations of the horizontal component of the geomagnetic field, filtered from the series $H(t)$ in the range of periods of 2–20 min (c), (d) distribution $N(t)$ of the number of TWPs detected on that day for all stations of the global GPS network used in the analysis, with the rms higher than $\varepsilon = 0.1$ *TECU*; (e) dynamic amplitude spectrum of TEC variations in the range of periods of 5–60 min obtained through a spatial averaging of the spectra for the entire California region (220–260°E; 28–42°N).

fluctuations yet cannot cause large-scale changes in electron density characteristic for a geomagnetically disturbed ionosphere.

Geomagnetic field *Dst*-variations for October 18, 2001 are plotted in Fig. 6a. In the analysis of the geomagnetic situation we used also the data from magnetic observatory Victoria (48.52°N; 236.58°E) where for the time interval of our interest a weak geomagnetic disturbance was recorded, which implied a decrease of the horizontal component $H(t)$ of the magnetic field by 60 nT (Fig. 6b). There was a concurrent, small decrease of the fluctuation amplitude of the $\mathrm{d}H(t)$-component in the range of periods 2–20 min (Fig. 6c). The range of variation of the geomagnetic *Dst*-index (Fig. 6a) for the selected time interval was also relatively small (no more than 20 nT), yet the period 15:30–18:00 UT showed a clearly pronounced decrease of the *Dst*-index coinciding with the period of the decrease of the H-component of the magnetic field (Fig. 6b).

Fig. 6d presents the distribution $N(t)$ of the number of TWPs detected for that day by all stations of the global GPS system analyzed here, with the rms in excess of $\varepsilon = 0.1$ *TECU*. Fig. 6e illustrates the dynamic amplitude spectrum $S(f, t)$ of TEC variations in the range of periods 5–60 min obtained by using the method of spatial averaging of the spectra for the entire California region (Afraimovich et al., 2001b).

Overall, the TEC variations correlate with geomagnetic field variations (see Discussion). Between 15:00 and 19:00 UT, the enhancement of the oscillations of the H-component was accompanied by an expansion of the spectrum and by an increase of the TEC fluctuation amplitude. The highest intensity is shown by the TEC oscillations with periods of 12–17 min between 15:30 and 17:00 UT. The largest number of TWPs was also recorded during the same period of time (Fig. 6d).

To check that TWPs were observed on that day somewhere else on the globe and not only between 15:00 and 19:00 UT, we processed the data with different values of the threshold ε for the entire global GPS network.

Fig. 7 presents the sample statistics of the TWPs identified for October 18, 2001 as a function of UT and local time LT, calculated for the longitude of 240°E corresponding to the middle of the California region: Fig. 7a—from TWPs with the rms higher than $\varepsilon = 0.1$ *TECU* obtained from all stations of the global GPS network used in the study (copy of Fig. 6d); Figs. 7b and c—same as in Fig. 7a but for $\varepsilon = 0.05$ *TECU* and $\varepsilon = 0.01$ *TECU*; Fig. 7d—rms higher than $\varepsilon = 0.01$ *TECU* for the data from the California region only.

An analysis of the Fig. 7 data leads us to conclude that the TWPs on that day were observed mainly in California only and only over the time interval 15:00–17:00 UT.

4.2. *Methods of determining the form and dynamic characteristics of TWPs*

The methods of determining the form and dynamic characteristics of TIDs that are used in this study are based on those reported in (Mercier, 1986; Afraimovich, 1997; Afraimovich et al., 1998, 1999, 2000a,b).

We determine the velocity and direction of motion of the phase interference pattern (phase front) in terms of some model of this pattern, an adequate choice of which is of critical importance. In the simplest form, space–time variations in phase of the transionospheric radio signal that are proportional to TEC variations $I(t, x, y)$ in the ionosphere, at each given time t can be represented in terms of the phase interference pattern that moves without a change in its shape

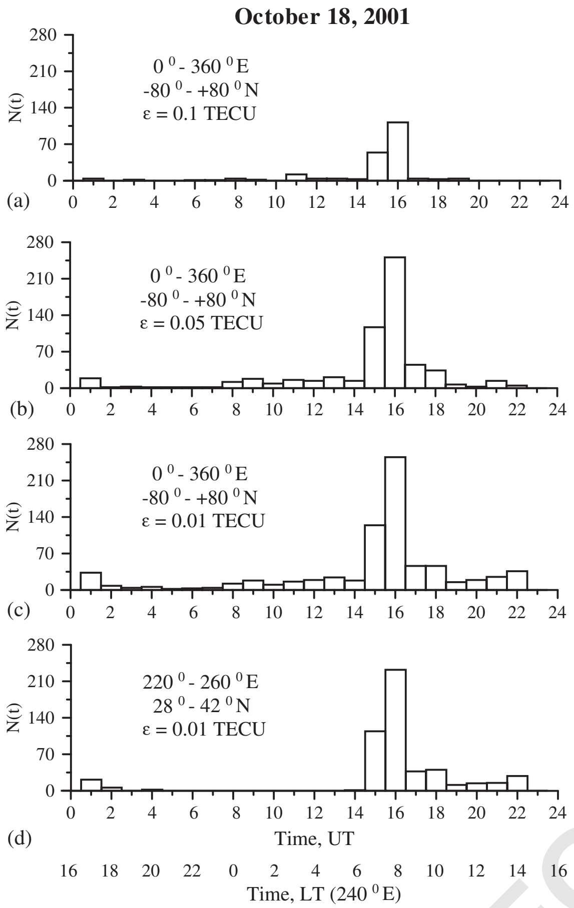

Fig. 7. Number $N(t)$ of TWPs of October 18, 2001 as a function of UT and local time LT, calculated for the longitude of 240°E, corresponding to the middle of the California region: (a) from TWPs with the rms higher than $\varepsilon = 0.1$ *TECU* obtained for all stations of the global GPS network used in the analysis (copy of Fig. 6d); (b) and (c) same as in panel (a) but for $\varepsilon = 0.05$ *TECU* and 0.01 *TECU*; (d) with the rms higher than $\varepsilon = 0.01$ *TECU* according to the data from the California region only (220–260°E; 28–42°N).

(the non dispersive disturbances):

$$I(t,x,y) = F\left(t - \frac{x}{u_x} - \frac{y}{u_y}\right), \tag{4}$$

where $u_x(t)$ and $u_y(t)$ are the velocities of intersection of the phase front of the axes x (directed to the East) and y (directed to the North), respectively.

A special case of Eq. (4) is the most often used model for a solitary, plane travelling wave of TEC disturbance:

$$I(t,x,y) = \delta \sin(\Omega t - K_x x - K_y y + \varphi_0), \tag{5}$$

where $I(t,x,y)$ are space–time variations of TEC; $\delta(t) = \exp[-((t - t_{\max})/(t_{\mathrm{d}}))^2]$—the amplitude; K_x, K_y, Ω are the x- and y-projections of the wave vector $\boldsymbol{K}$, and the angular frequency of the disturbance, respectively; φ_0 is the initial disturbance phase; $t_{\max}$ is the time when the disturbance has a maximum amplitude; t_{d} is the half-thickness of the wave packet. On Fig. 1 α, θ are azimuth and elevation of the wave vector of TID $\boldsymbol{K}_t$, $\boldsymbol{K}$ is horizontal projection of $\boldsymbol{K}_t$.

It should be noticed, however, that in real situations neither of these ideal models (4) and (5) are realized in a pure form. This is because that the TIDs propagate in the atmosphere in the form of a dispersing wave packet with a finite value of the width of the angular spectrum. But in the first approximation on short time interval of averaging compared to time period of filtered variations of TEC, the phase interference pattern moves without a substantial change in its shape.

Mercier (1986) suggested a statistical method to analyze the phase interference pattern. Primary data comprise time dependencies of the spatial phase derivatives $I'_y(t)$ and $I'_x(t)$ along the directions y and x. Method of Mercier (1986) involves determining a series of instantaneous values of the direction $\alpha(t)$

$$\alpha(t) = \arctan(I'_x(t)/I'_y(t)) \tag{6}$$

and constructing subsequently, on a chosen time interval, the distribution function of azimuth $P(\alpha)$. The central value of α is used by Mercier (1986) as an estimate of the azimuth of prevailing propagation of TIDs (modulo 180°).

The other method is based on analyzing the phase interference pattern anisotropy in the antenna array plane by determining the contrast C of the interference pattern (Mercier, 1986). In this case the ratio $C_{x,y}$ is calculated as follows:

$$C_{x,y} = \sigma_X/\sigma_Y \quad \text{if } \sigma_X > \sigma_Y,$$

$$C_{x,y} = \sigma_Y/\sigma_X \quad \text{if } \sigma_Y > \sigma_X, \tag{7}$$

where X and Y are series of the transformed values of $I'_x(t)$ and $I'_y(t)$ obtained by rotating the original coordinate system (x, y) by the angle β:

$$X(t) = I'_x(t)\sin\beta + I'_y(t)\cos\beta,$$

$$Y(t) = -I'_x(t)\cos\beta + I'_y(t)\sin\beta \tag{8}$$

and σ_X and σ_Y are rms of the corresponding series.

Mercier (1986) showed that it is possible to find such a value of the rotation angle β_0, at which the ratio $C_{x,y}$ will be a maximum and equal to the value of contrast C. This parameter characterizes the degree of anisotropy of the phase interference pattern. The angle β_0 in this case indicates the direction of elongation, and the angle $\alpha_c = \beta_0 + \pi/2$ indicates the direction of the wave vector $\boldsymbol{K}$ coincident (modulo 180°) with the propagation direction of the phase front.

The method of Mercier (1986) essentially makes it possible to determine only the anisotropy and the direction of irregularity elongation of the phase interference pattern (modulo 180°).

A statistical, angle-of-arrival and Doppler method (SADM) was proposed by Afraimovich (1997) for determining the characteristics of the dynamics of the phase interference pattern in the horizontal plane by measuring variations of phase derivatives with respect not only to the spatial coordinates $I'_x(t)$ and $I'_y(t)$ proportional to angle-of-arrival variations, but additionally to the time $I'_t(t)$ proportional to frequency Doppler shift variations. This permits the determination of the unambiguous orientation $\alpha(t)$ of the wave vector $\boldsymbol{K}$ in the range 0–360° and the horizontal velocity $V_h(t)$ at each specific instant of time.

Afraimovich et al. (1998, 2000b) described the updating of the SADM algorithm for GPS-arrays (SADM-GPS) based on a simple model for the displacement of the phase interference pattern that travels without a change in the shape and on using current information about the angular coordinates of the GPS satellites: the elevation $\theta_s(t)$ and the azimuth $\alpha_s(t)$. Of course, such an approximation is acceptable only for large values of the LOS elevation θ_s.

The method SADM-GPS makes it possible to determine the horizontal velocity $V_h(t)$ and the azimuth $\alpha(t)$ of TID displacement at each specific instant of time (the wave vector orientation $\boldsymbol{K}$) in a fixed coordinate system (x, y):

$$\alpha(t) = \arctan(I'_x(t)/I'_y(t)),$$
$$u_x(t) = I'_t(t)/I'_x(t) = u(t)/\sin\alpha(t),$$
$$u_y(t) = I'_t(t)/I'_y(t) = u(t)/\cos\alpha(t),$$
$$u(t) = |u_x(t)u_y(t)|/(u_x^2(t) + u_y^2(t))^{1/2},$$
$$V_h(t) = u(t) + w_x(t)\sin\alpha(t) + w_y(t)\cos\alpha(t), \tag{9}$$

where u_x and u_y are the propagation velocities of the phase front along the axes x and y in a frame of reference related to the GPS-array; w_x and w_y are the x and y projections of the velocity w of the subionospheric point (for taking into account the motion of the satellite).

The coordinates of the subionospheric point $x_s(t)$ and $y_s(t)$ at h_{max} in the chosen topocentric coordinate system vary as

$$x_s(t) = h_{max}\sin(\alpha_s(t))ctg(\theta_s(t)),$$
$$y_s(t) = h_{max}\cos(\alpha_s(t))ctg(\theta_s(t)) \tag{10}$$

and the x- and y-components of the displacement velocity w:

$$w_x(t) = \mathrm{d}x_s(t)/\mathrm{d}t,$$
$$w_y(t) = \mathrm{d}y_s(t)/\mathrm{d}t,$$
$$w(t) = (w_x^2(t) + w_y^2(t))^{1/2}. \tag{11}$$

Let us take a brief look at the sequence of data handling procedures. Out of a large number of GPS stations, three points (A–C) are chosen in such a way that the distances between them do not exceed about one-half the expected wavelength Λ of the disturbance (see Fig. 1). The point B is taken to be the center of a topocentric frame of reference. Such a configuration of the GPS receivers represents a GPS-array (or a GPS-interferometer) with a minimum of the necessary number of elements. In regions with a dense network of GPS-points, we can obtain a broad range of GPS-arrays of a different configuration, which furnishing a means of testing the data obtained for reliability; in this paper we have taken advantage of this possibility.

The input data include series of the vertical TEC $I_A(t)$, $I_B(t)$, $I_C(t)$, as well as corresponding series of values of the elevation $\theta_s(t)$ and the azimuth $\alpha_s(t)$ of the LOS.

Series of the values of the elevation $\theta_s(t)$ and azimuth $\alpha_s(t)$ of the LOS are used to determine the location of the subionospheric point, as well as to calculate the elevation θ of the wave vector $\boldsymbol{K}_t$ of the disturbance from the known azimuth α (see formula (14)).

Since the distance between GPS-array elements (from several tens to a few hundred of kilometers) is much smaller than that to the GPS satellite (over 20,000 km), the array geometry at the height near the main maximum of the F_2-layer is identical to that on the ground.

Linear transformations of the differences of the values of the filtered TEC $(I_B - I_A)$ and $(I_B - I_C)$ at the receiving points A–C are used to calculate the components of the spatial TEC gradients I'_x and I'_y (Afraimovich et al., 1998)

$$I'_x = [y_A(I_B - I_C) - y_C(I_B - I_A)]/[x_A y_C - x_C y_A], \tag{12}$$

$$I'_y = [x_C(I_B - I_A) - x_A(I_B - I_C)]/[x_A y_C - x_C y_A], \tag{13}$$

where x_A, y_A, x_C, y_C are the coordinates of the sites A and C in the topocentric coordinate system. When deriving Eqs. (12) and (13) we took into account that $x_B = y_B = 0$, since site B is the center of topocentric coordinate system (see Fig. 1).

The time derivative of TEC I'_t is determined by differentiating $I_B(t)$ at the point B.

The resulting series are used to calculate instantaneous values of the horizontal velocity $V_h(t)$ and the azimuth $\alpha(t)$ (clockwise, $\alpha = 0$ in direction North) of TID propagation. Next, the series $V_h(t)$ and $\alpha(t)$ are put to a statistical treatment. This involves constructing distributions of the horizontal velocity $P(V_h)$ and direction $P(\alpha)$ which are analyzed to test the hypothesis of the existence of the preferred propagation direction. If such a direction does exist, then the corresponding distributions are used to calculate the mean value of the horizontal velocity $\langle V_h \rangle$, as well as the mean value of the azimuth $\langle \alpha \rangle$ of TID propagation.

As a first approximation, the transionospheric sounding method is responsive only to TIDs with the wave vector $\boldsymbol{K}_t$ perpendicular to the direction $\boldsymbol{r}$ of the LOS (Afraimovich et al., 1992). A corresponding condition for elevation θ and azimuth α has the form

$$\tan\theta = -\cos(\alpha_s - \alpha)/\tan\theta_s. \tag{14}$$

Hence, the phase velocity V can be defined as

$$V = V_h\cos(\theta). \tag{15}$$

The aspect dependence (14) of the TEC disturbance amplitude is of significant importance for investigating wave disturbances. Condition (14) imposes a constraint on the number of LOSs for which a reliable detection of TIDs at the background of noise is possible. The aspect effect causes the disturbance maximum to be displaced along the time axis, which can introduce errors in determining the TID displacement if the velocity is calculated from time delays. Furthermore, as will be shown below, the aspect effect will give rise to structures of the type of wave packets "observed" in TEC variations, which do not exist in the reality.

Afraimovich et al. (1992) showed that for the Gaussian ionization distribution the TEC disturbance amplitude M is determined by the aspect angle γ between the vectors $\boldsymbol{K}_t$ and direction $\boldsymbol{r}$ along LOS to the satellite (see Fig. 1), as well as by the ratio of the wavelength of the disturbance Λ to the half-thickness of the ionization maximum h_d:

$$M(\gamma) \sim \frac{h_\mathrm{d}}{\sin(\theta_\mathrm{s})} \exp\left[-\left(\frac{\pi h_\mathrm{d}\cos(\gamma)}{\Lambda \sin(\theta_\mathrm{s})}\right)^2\right]. \tag{16}$$

In this paper the influence of aspect effects on the character of TEC behavior and on the accuracy of the calculated parameters of TWPs was investigated and the reliability of the determination of TWP characteristics was verified by modeling the wave disturbances of electron density for the observing conditions of October 18, 2001.

Thus, on the basis of using the transformations described in this section, for each of the GPS arrays chosen for the analysis we obtained the average (for the time interval of about 1–2 h) values of the following TWP parameters: $\langle A_I \rangle$, the amplitude of the TEC disturbance; $\langle \alpha \rangle$ and $\langle \theta \rangle$—the azimuth and elevation of the wave vector $\boldsymbol{K}_t$, $\langle V_\mathrm{h} \rangle$ and $\langle V \rangle$—the horizontal component and the phase velocity modulus, the contrast C, and the azimuth of a normal to the wave front α_c from the method reported by Mercier (1986).

4.3. Dynamic characteristics of TWP

Fig. 8a plots the typical time dependencies of TEC $I(t)$ for GPS satellite PRN14 for three GPS stations: BRAN, CHMS, and DUPS in California. The three GPS sites constitute a typical GPS array, the data from which were processed by the technique described in the preceding section. For the same stations Fig. 8b presents the TEC variations $\mathrm{d}I(t)$ that were filtered from the initial series $I(t)$ using the band-pass filter with the boundaries from 5 to 20 min.

The filtered series for the period 15:00–16:00 UT show the presence of significant TEC oscillations of the type of single wave packet with a duration of about 1 h and with the amplitude $A = 0.5$ $TECU$. Not only does the range of the filtered oscillations $\mathrm{d}I(t)$ far exceed the error of phase measurements (10^{-3} $TECU$), but it also exceeds nearly an order of magnitude the level of background TEC variations. TEC variations from the three spatially separated GPS stations show a high degree of similarity and have a small time shift. This suggests that we are dealing here with the same traveling disturbance.

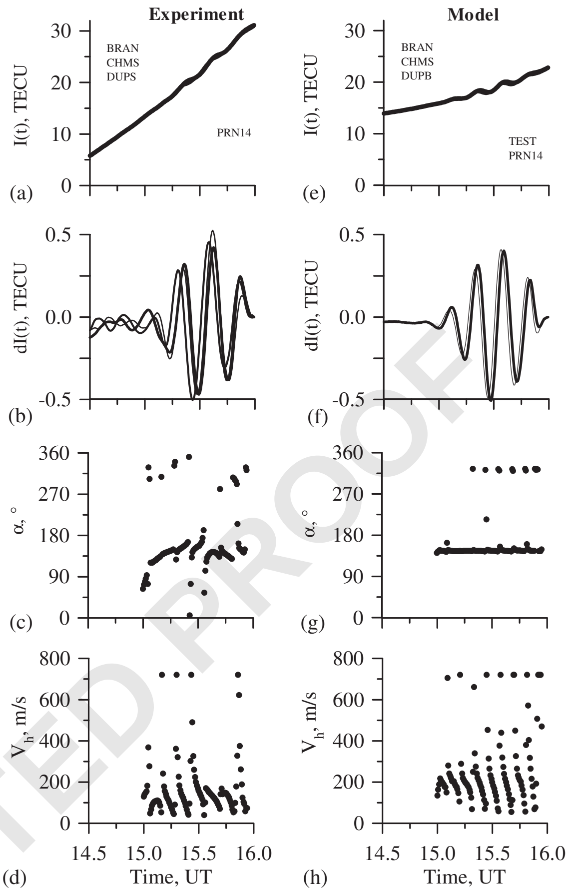

Fig. 8. Time dependencies of the initial TEC series $I(t)$—panels (a,e) and filtered TEC series $\mathrm{d}I(t)$–(b,f); directions α of the wave vector $\boldsymbol{K}$–(c,g) and of the modulus of the horizontal velocity V_h of TWP–(d,h), determined for the GPS array (BRAN, CHMS, DUPS) using the SADM-GPS method. Panels (a–d) present the experimental data, and panels (e–h) show the calculated data for the TWP model in the form of a single wave packet.

Results of a calculation (using the SADM-GPS algorithm) of the mean values of the azimuth $\langle \alpha \rangle$ and the horizontal velocity $\langle V_\mathrm{h} \rangle$ of the disturbance for each 30-s time interval are presented in Figs. 8c and d. As is evident from the figure, this wave packet was traveling predominantly in the south-eastward direction with the mean velocity of about 180 m/s. The scatter of the counts is caused by the incomplete correspondence of the actual picture of an ideal TWP model in the form of a monochromatic packet (5) and, in particular, by the presence of background non-correlated TEC fluctuations (Afraimovich et al., 1998).

A processing of the data from the other GPS arrays in the same region (Fig. 5c) by use of the SADM-GPS method provided distributions of the main TWP parameters recorded on October 18, 2001 in California. The various combinations of GPS arrays for the time interval 15:00–16:00 UT totaled

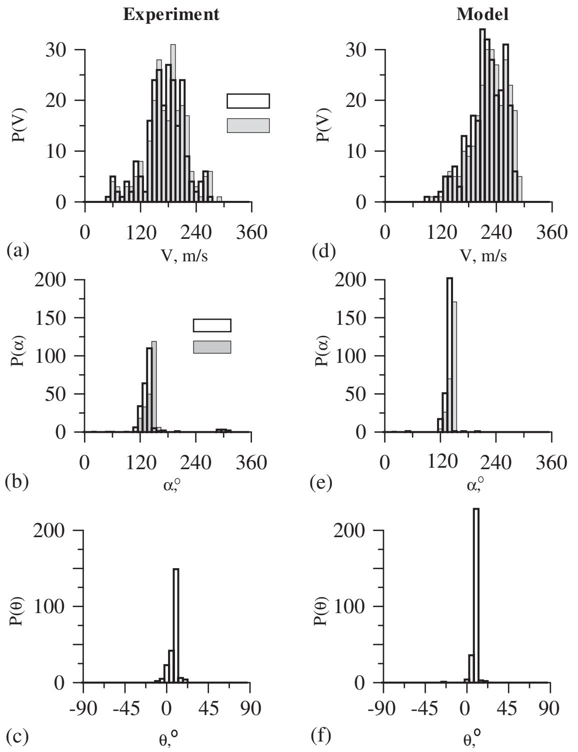

Fig. 9. Distributions of the TWP parameters as determined by the SADM-GPS method: (a,d) modulus (clear bar) and horizontal component (painting bar) of the TWP phase velocity; (b,e) azimuth (clear bar); (c,f) elevation of the TWP wave vector. Panels (b) and (e) present also the distributions of the TWP propagation azimuth calculated from the contrast (painting bar). Panels (a–c) present the experimental data, and panels (d–f) show the calculated data for the TWP model in the form of a single wave packet.

231. Statistical data show an agreement of the mean values of the calculated parameters to within their rms, which indicates a good stability of the data obtained, irrespective of the particular configuration of a GPS array.

Distributions of the mean values of the TWP parameters calculated for each of the 231 GPS arrays are presented in Figs. 9a–c. According to our data, the value of the horizontal propagation velocity V_h of TWP (Fig. 9a) varies from 40 to 290 m/s, with the most probable value 190 m/s. The TWP wavelength Λ with the mean oscillation period of about 1000 s is on the order of 150–200 km.

An analysis of the distribution of the azimuths $P(\alpha)$ (Fig. 9b) shows a clearly pronounced south-eastward direction of TWP displacement $140 \pm 20°$. The average (for 231 GPS arrays) value of the contrast $C = 7$ suggests a strong anisotropy of TWPs. Fig. 9b shows also the distribution of the azimuth of a normal to the wave front $P(\alpha_c)$ deduced by the method of Mercier (1986). This distribution virtually coincides with $P(\alpha)$, suggesting that the TWP travel across their elongation. Thus, the typical size of the entire wave packet along the propagation direction is about 300–500 km, and along the wave front it is as long as 1000 m.

The arrow in Fig. 5c schematically shows the wave vector $\boldsymbol{K}$ of the TWP. The values of α and V_h, presented in Fig. 5c, correspond to the most probable values of the propagation azimuth and the modulus of the horizontal velocity of the TWPs.

The elevation of the TWP wave vector, determined from the aspect condition (14), has mostly a small positive value about $+10°$ (Fig. 9c). Accordingly, estimations of the phase velocity V (Fig. 9a) give values close to the value of its horizontal projection 50–270 m/s, with the largest probable value 180 m/s.

4.4. Modeling

In this paper the influence of aspect effects on the character of TEC behavior and on the accuracy of the calculated of TWPs was investigated and the reliability of the determination of the TWP characteristics was verified by modeling the wave disturbances of electron density for the observing conditions of October 18, 2001.

Our developed model of TEC measurements with the GPS interferometer makes it possible to calculate as realistic a spatial and temporal distribution of the local electron density N_e in the ionosphere as possible and then, using the coordinates of the receiver sites and of the satellites, to integrate N_e along the receiver-satellite LOS with a given step over time (Afraimovich et al., 1998). As a result we obtain time series of TEC similar to input experimental data which can be processed by the same methods as used to process experimental data.

The ionization model takes into account the height distribution of N_e, the seasonal and diurnal density variations determined by the zenith angle of the Sun, as well as irregular disturbances of N_e of a smaller amplitude and smaller spatial scales in the form of a discrete superposition of plane traveling waves.

In this paper, with the purpose of elucidating the origin of TWP, three types of disturbances were modeled:

(a) the disturbance in the form of a single plane wave with amplitude $A_1 = 3\%$ in the ionization maximum, with the period $T_1 = 15$ min and the wavelength $L_1 = 172$ km. The elevation of the wave $\theta_1 = 10°$, and the azimuth $\alpha_1 = 146°$;
(b) the disturbance in the form of a superposition of two plane waves with periods $T_1 = 15$ min and $T_2 = 12$ min, and with the wavelengths $L_1 = 172$ km and $L_2 = 138$ km. The elevations, azimuths and azimuths of the waves were specified identical: $\theta_1 = \theta_2 = 10°$, $\alpha_1 = \alpha_2 = 146°$, $A_1 = A_2 = 3\%$ of the value of N_e in the ionization maximum;
(c) the disturbance in the form of a single wave packet, with the semi-thickness $t_d = 20$ min and a maximum amplitude at the time $t_{max} = 15.50$ UT. The oscillations

inside the packet had the period $T_1 = 15$ min and the wavelength $L_1 = 172$ km.

Disturbance parameters were taken to be close to those obtained from experimental data using the technique from Afraimovich et al. (1998). TWPs were modeled with the purpose of verifying the reliability of the calculated TWP characteristics, and elucidating the origin of TWPs. A detailed description of the model used is given in Afraimovich et al. (1998).

Figs. 8e–h (at the right) presents the results of calculations in terms of the model of the TWP in the form of a single wave packet for the BRAN, CHSM, DUPR array on October 18, 2001. Parameters of the wave packet were taken to be close to experimental data (Figs. 8a–d). Distributions of TWP parameters obtained in a similar modeling of TWP for the other California GPS arrays are presented in Figs. 9d–f (at the right).

Fig. 8 illustrates a good similarity of the experimental and model TEC variations $I(t)$, d$I(t)$ and the dependencies $V_h(t)$ and $\alpha(t)$. Noteworthy is the weaker inclination of the model TEC $I(t)$ (Fig. 8e) when compared with the experimental one (Fig. 8a). This is because for the sake of simplicity and for illustrative purposes, diurnal variations in ionization in the model are proportional to the cosine of the zenith angle of the Sun. In actual conditions the dependence is more complicated, which gives a faster temporal growth of the TEC. Because the trend is removed in the subsequent discussion and only the relative TEC variations d$I(t)$ are considered, the above-mentioned difference in the behavior of the model and experimental TEC will not affect results obtained.

A comparison of the TEC disturbance parameters specified in the model with the corresponding values obtained following a processing by formulas of the SADM-GPS method shows a relatively good agreement of these values. The azimuth of the wave vector of TWP was taken to be $\alpha = 146°$, and the mean value of the azimuth calculated by the SADM-GPS method is 146.2° (Figs. 8g and c); the horizontal velocity was specified equal to 180 m/s, the calculated mean value of the velocity was 207.5 m/s (Figs. 8h and 9d).

The minor difference in the mean values of the phase velocity could be due to some inaccuracy of specification of model disturbance parameters. Besides, the model used here (Afraimovich et al., 1998) neglects the sphericity, which might affect modeling results even for relatively high elevations of the LOS to the satellite.

The elevation in the model was $\theta = 10°$, and the most probable value of the calculated elevation was 10° (Fig. 9f). The azimuth of TWP propagation determined by the SADM-GPS method was also close to the azimuth values calculated by analyzing the contrast of the phase interference pattern (Mercier, 1986)—Fig. 9e. All this demonstrates the validity of the SADM-GPS technique and confirms the reliability of the TWP parameters obtained using this technique.

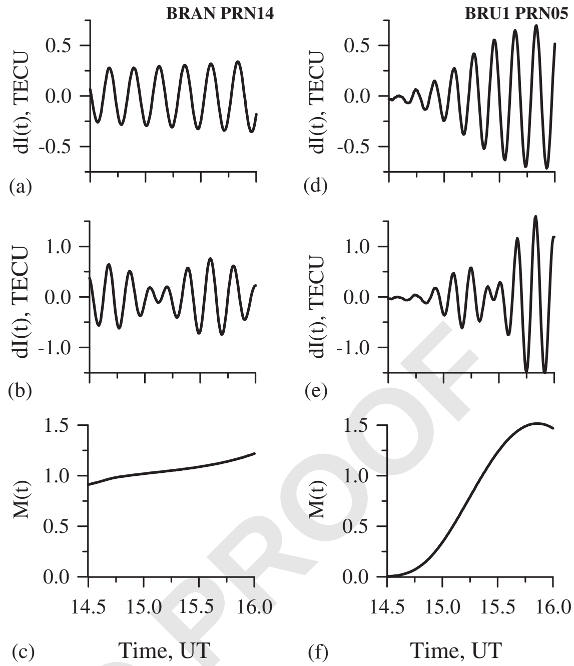

Fig. 10. Time dependencies of the filtered TEC series d$I(t)$, calculated for the TID model in the form of a single plane wave (a,d) and in the form of a superposition of two plane waves (b,e). Panels (c,f) present the theoretical dependencies of the TEC response amplitude $M(t)$. On the left—calculations for the GPS PRN14 satellite at the BRAN site; on the right—for the PRN05 satellite at the BRU1 site.

Let us now consider the possible mechanisms that are responsible for the formation of structures of the type of TWP in observed TEC variations. The recorded TWP represents a single wave packet with a duration of about 60 min, the oscillation period inside the packet of 12–15 min, and with the amplitude exceeding the level of background fluctuations by a factor of 10 (Fig. 8b). Structures of such a type can be produced in TEC variations in different ways.

If a monochromatic wave with a period of about 15 min (the period of observed TEC variations) propagates in the ionosphere, then TEC oscillations of the type of TWP could be produced through the aspect effect. Figs. 10 a and d illustrates such a situation. Panels (a) and (d) present the filtered TEC series obtained by modeling a single plane wave under different conditions of its observation. At the BRAN site (Fig. 10a) the elevations of the PRN14 satellite are close to 90°, and the wave vector of the disturbance is perpendicular to the receiver-satellite LOS throughout the observing period. This is indicated by the character of the theoretical dependence $M(t)$ calculated by formula (16) for this LOS: $M(t)$ is close to 1 over the entire observing interval (Fig. 10c). Waves disturbances of the TEC close to the specified monochromatic wave are therefore observed along the BRAN-PRN14 LOS.

At the BRU1 site for PRN05, the detection conditions for disturbances are significantly worse. In this case for the first half an hour the wave propagates virtually along the LOS ($M(t) < 0.3$, Fig. 10f), and at the end of the observing interval the BRU1-PRN15 LOS is perpendicular to the propagation direction of the wave but has low elevations ($M(t) > 1$, Fig. 10f). Owing to this, TEC variations show an increase in the oscillation amplitude from 0 to 0.7 *TECU*—there arises a feature resembling a wave packet that was absent in the initial specified model of the wave. However, as is evident from the figure, in this case the increase in the TEC variation amplitude has an almost linear character while the experiment (Fig. 8b) shows a nonlinear amplitude modulation.

An investigation of the character of the aspect dependence for all GPS arrays that were used in this study, showed that in 97% of cases (including those shown in Fig. 8b) the situation is realized, which is depicted in Fig. 10c, i.e. $M(t)$ is close to 1 throughout this observing interval. Considering all that has been said above, one can draw the conclusion that the recorded TWPs are indeed caused by the propagation of an actual wave packet of a local density disturbance in the ionosphere rather than resulting from the recording conditions.

Another possibility of the production of a TWP is the combination of two or several monochromatic waves with close periods propagating in the ionosphere (Yakovets et al., 1999). We modeled the propagation of two quasi-horizontal waves with periods $T_1 = 15$ min and $T_2 = 12$ min by identical amplitudes, velocities and directions of propagation. The resulting TEC variations along two LOS: BRAN-PRN14, and BRU1- PRN05, with the trend removed, are presented in Figs. 10b and e, respectively.

As would be expected, there arise amplitude-modulated TEC oscillations with the modulation period of about $T = T_1T_2/(T_2 - T_1) = 60$ min. The period is close to the length of the wave packet recorded experimentally; however, a simple superposition of two waves gives not one but a whole chain of wave packets. In the case where the aspect sensitivity affects little the character of TEC variations (Fig. 10c) these packets have, in addition, different amplitudes as well (Fig. 10b). A phase change of the combined waves affects little the picture presented here by altering the form and position of the amplitude minimum only slightly. The aspect dependence in Fig. 10f, however, introduces an additional modulation into the recorded signal—there occurs a significant enhancement of one of the chain's packets (Fig. 10e), and the picture approaches what is observed experimentally in Fig. 8b.

Nevertheless, it cannot be believed that the observed single TWPs are the result of the aspect effect. Firstly, in the case of the aspect modulation, because of the slow (nearly linear) change of the amplitude, not one but at least two wave packets are observed. Secondly, as has been pointed out above, the character of the aspect dependence in most cases of TWP recordings was such that it affected little the amplitude of disturbances. To obtain the closets TEC oscillations to those observed experimentally we had to introduce an artificial modulation, i.e. the amplitude of the initial monochromatic wave of the disturbance N_e was specified not constant but it had a time dependence in the form of a Gaussian function. It is such a model of TEC variations that is shown in Fig. 8f.

5. Discussion of results

Let us discuss of our results and compare it with the findings reported by other authors.

Our estimate of the radius of spatial correlation (on the order of several hundred kilometers) is in reasonably good agreement with the data reported by Yakovets et al. (1999).

Yakovets et al. (1999) argued that the observed wave packets are the superposition of the direct and ground-reflected wave whose source lies in the troposphere. The analysis made in this paper (Section 4.4) did not confirm the validity of such an explanation for the October 18, 2001 TWPs.

By comparing our detected TWPs with the data from (Yakovets et al., 1999; Hines, 1960; Waldock and Jones, 1984; Francis, 1974) as well as with the findings of our modeling, it can be assumed that in the atmosphere there exists an additional amplitude modulation mechanism for wave processes which makes it possible to obtain closest TEC oscillations in the form of a single wave packet.

Francis (1974), by considering the auroral electrojet to be the source of TIDs, showed that upon propagating through the atmosphere into the F-region, the ground-reflected waves acquire the properties of a wave packet. However, the October 18, 2001 case that is considered in detail in this paper refers to the mid-latitude region and to a sufficiently magnetically quiet period when the conditions of realization of the Francis's mechanism are not satisfied.

Our data on the TWP climatology and TWP displacement velocity and direction correspond to those of mid-latitude medium-scale traveling ionospheric disturbances obtained previously in the analysis of phase characteristics of HF radio signals (Kalikhman, 1980; Waldock and Jones, 1984, 1986, 1987; Jacobson and Carlos, 1991), as well as signals from first-generation navigation satellites (Spoelstra, 1992), geostationary satellites (Afraimovich et al., 1999; Jacobson et al., 1995) and discrete space radio sources (Mercier, 1986, 1996; Velthoven et al., 1990).

Our values of the periods, relative amplitude and of the displacement direction of MSTIDs are in the closest agreement with the data reported by Spoelstra (1992) and Velthoven et al. (1990).

The elevation of the TWP wave vector has mostly a small positive value about $+10^\circ$ (Fig. 9c). It can be assumed that the TWP represent an almost horizontal wave. Such a small value of the elevation gives no way of deducing (with the necessary reliability) the degree of correspondence of the phase propagation direction to gravity wave theory (upward or downward) (Hines, 1960; Francis, 1974).

What are the mechanisms of generation of MS AGW or the propagation conditions in the atmosphere which give rise to such wave packets?

Some authors associate the variations of the frequency Doppler shift F_D with MSTIDs that are generated during the passage of atmospheric fronts, tornadoes, and hurricanes (Baker and Davies, 1969; Bertin et al., 1975, 1978; Hung et al., 1978; Kersly and Rees, 1982; Stobie et al., 1983; Huang et al., 1985).

On the basis of the dispersion relation Hines (1960), Waldock and Jones (1984) showed that TIDs that are associated with a tropospheric jet flow occur in the F-region in the form of a wave packet with quasi-monochromatic oscillations, the period of which is a function of inclination angle of the wave vector during the propagation of the wave from the source to the place of observation in the F-region.

However, our data do not permit us to establish a direct correlation between the occurrence of TWP and corresponding meteorological phenomena. Also, we did not obtain any confirmation of the effectiveness of the mechanism of generation of MSTIDs as a consequence of the movement of the solar terminator (Somsikov, 1995). On the contrary, the diurnal dependence of the TWP occurrence (Fig. 4b) indicates that the most probable time of TWP recording is local noon.

Periodic electron density oscillations of the type of wave packets were investigated previously in terms of the hypothesis of their association with geomagnetic field pulsations (GP). Geomagnetic pulsations represent natural electromagnetic oscillations which are recorded as variations of the electric field (telluric currents). GP are characterized by a quasi-periodic structure and occupy the range from a few thousandths to several Hz. It is believed that geomagnetic pulsations are inherently magnetohydrodynamic (MHD) waves excited in the magnetosphere.

The greater part of evidence of the association between GP and periodic electron density oscillations in the ionosphere was obtained by recording the frequency Doppler shift if the ionosphere-reflected radio signal (Rishbeth and Garriot, 1964; Klostermeyer and Rottger, 1976; Duffus and Boyd, 1968; Al'perovich et al., 1991) and TEC variations measured using signals from geostationary satellites (Davies and Hartmann, 1976; Okuzawa and Davies, 1981).

However, many years of investigations have not yet provided thorough insight into the mechanisms accounting for the linkage between GP and ionospheric variations. One reason for that is the difficulty associated with obtaining statistically significant sets of experimental data.

The other reason is the difference of characteristic spatial scales of TEC disturbances and geomagnetic pulsations. Attempts to use GPS data in tackling this problem have already been made (for instance, by Potapov et al., 2002), yet results derived from investigating the correlation between TEC pulsations and geomagnetic pulsations are still unsatisfactory. In this paper, we did not obtain any direct confirmation for the correlation of these phenomena either.

Medium-scale TEC disturbances are an important factor that determines the performance of the GPS system itself.

Recent years saw extensive studies of phase fluctuations, phase slips of range measurements and error of positioning accuracy of GPS receivers in conditions of geomagnetic disturbances (Afraimovich et al., 2001a, 2002, 2003; Skone and de Jong, 2000, 2001; Coster et al., 2001; Shan et al., 2002).

Afraimovich et al. (2001a, 2002) found that during magnetic storms, the relative density of phase slips at mid latitudes exceeds its mean value for magnetically quiet days at least by the order of one or two, and reaches a few percent of the total density of observations. Furthermore, the level of phase slips for the GPS satellites located at the sunward side of the Earth was 5–10 times larger compared with the opposite side of the Earth.

Afraimovich et al. (2003) found, that during magnetic storms the errors of positioning for two-frequency GPS receivers of three main types (Ashtech, Trimble, and AOA) increases at least by the order of one or two.

There are the high positive correlation between the growth of the density of phase slips and the intensity of TEC variations in SM TID time periods, 10–60 min (Afraimovich et al., 2001a, 2002). These results are in reasonably good agreement with data reported by Coster et al. (2001).

As a result of these investigations, it has become clear that ionospheric disturbances during magnetic storms contribute to signal degradation and GPS system malfunctions not only at the equator and in the polar zone but also even at mid-latitudes.

A detailed analysis of the factors responsible for the degradation of the GPS performance during magnetic storms is a highly difficult task, and is beyond the scope of this paper.

6. Conclusions

Main results of this study may be summarized as follows:

1. The method of GPS interferometry of MSTIDs has been developed that opens up a new era in the studies of the TID morphology and climatology. For the first time, the morphology of TWPs is presented for 105 days from the time interval 1998–2001 with a different level of geomagnetic activity, with the number of stations of the global GPS network ranging from 10 to 300. The TEC series used in the analysis are in total about 700,000.
2. TWPs in the time range represent quasi-periodic oscillations of TEC of a length on the order of 1 h with the oscillation period in the range 10–20 min and the amplitude exceeding the amplitude of "background" TEC fluctuations by one order of magnitude.

3. The most of the TWPs are observed during the daytime in no more than 0.1–0.4% of the total number of TEC series, most commonly in winter and autumn. There is no significant correlation between the TWP occurrence probability and values of the geomagnetic disturbance index *Dst*. The distance between any two GPS stations where the TWPs within a single 2.3-h time interval were observed does not exceed 500 km.
4. The dynamical parameters of the TWPs observed on October 18, 2001 over California, USA were determined. The TWPs traveled with the elevation $\theta = 10^\circ$ and the azimuth $\alpha = 146^\circ$. Its mean velocity $\langle V \rangle = 180$ m/s corresponds to the velocity of medium-scale AGWs.

Thus, according to our data, TWPs constitutes a specific case of the manifestation of MS AGWs. What mechanisms of generation of MS AGWs or what propagation conditions in the atmosphere give rise to such wave packets remains an open question, beyond the scope of this paper.

In the future it is planned to use to aforementioned method of GPS interferometry of MSTIDs to obtain more thorough information about the physical origin and climatology of MSTIDs for different geophysical conditions. In particular, we intend to estimate the generation effectiveness of MSTIDs in terms of our proposed mechanisms (movement of the solar terminator, meteorological phenomena, geomagnetic pulsations), as well as to undertake—on the new experimental basis—a verification of the well-known hypothesis of MSTID filtering by the neutral wind along the propagation direction.

Such investigations must have a comprehensive character, with the maximum possible involvement of experimental ionospheric monitoring facilities (digisondes, incoherent scatter radars, chirp-ionosondes, etc.).

Acknowledgements

We are indebted to Dr. A.S. Potapov for participating in discussions. We thank O.S. Lesyuta for help in organizing the experiment. We are also grateful to V.G. Mikhalkovsky for his assistance in preparing the English version of the manuscript. Finally, the authors wish to thank the referees for valuable suggestions which greatly improved the presentation of this paper. This work was done under state support grant No. Nsh-272.2003.5 for Leading Scientific Schools of the Russian Federation as well as Russian Foundation for Basic Research Grants Nos. 00-05-72026 and 03-05-64100. We acknowledge the Scripps Orbit and Permanent Array Center (SOPAC) for providing GPS data used in this study.

References

Afraimovich, E.L., 1997. Statistical angle-of-arrival and doppler method (SADM) for determining characteristics of the dynamics of the transionospheric radio signal interference pattern. Acta Geod. Geoph. Hung. 32 (3–4), 461–468.

Afraimovich, E.L., 2000. The GPS global detection of the ionospheric response to solar flares. Radio Science 35 (6), 1417–1424.

Afraimovich, E.L., Terekhov, A.I., Udodov, M.Yu., Fridman, S.V., 1992. Refraction distortions of transionospheric radio signals caused by changes in a regular ionosphere and by travelling ionospheric disturbances. Journal of Atmospheric and Solar-Terrestrial Physics 54, 1013–1020.

Afraimovich, E.L., Palamartchouk, K.S., Perevalova, N.P., 1998. GPS radio interferometry of travelling ionospheric disturbances. Journal of Atmospheric and Solar-Terrestrial Physics 60, 1205–1223.

Afraimovich, E.L., Boitman, O.N., Zhovty, E.I., Kalikhman, A.D., Pirog, T.G., 1999. Dynamics and anisotropy of traveling ionospheric disturbances as deduced from transionospheric sounding data. Radio Science 34 (2), 477–487.

Afraimovich, E.L., Kosogorov, E.A., Leonovich, L.A., Palamarchouk, K.S., Perevalova, N.P., Pirog, O.M., 2000a. Determining parameters of large-scale traveling ionospheric disturbances of auroral origin using GPS-arrays. Journal of Atmospheric and Solar-Terrestrial Physics 62, 553–565.

Afraimovich, E.L., Palamartchouk, K.S., Perevalova, N.P., 2000b. Statistical angle-of-arrival and doppler method for GPS interferometry of TIDs. Advances of Space Research 26 (6), 1001–1004.

Afraimovich, E.L., Lesyuta, O.S., Ushakov, I.I., Voeykov, S.V., 2001a. Geomagnetic storms and the occurrence of phase slips in the reception of GPS signals. Annals of Geophysics 45 (1), 55–71.

Afraimovich, E.L., Kosogorov, E.A., Lesyuta, O.S., Yakovets, A.F., Ushakov, I.I., 2001b. Geomagnetic control of the spectrum of traveling ionospheric disturbances based on data from a global GPS network. Annales Geophysicae 19 (7), 723–731.

Afraimovich, E.L., Lesyuta, O.S., Ushakov, I.I., 2002. Geomagnetic disturbances, and the GPS operation. Geomagnetism and Aeronomy 42 (2), 220–227.

Afraimovich, E.L., Demyanov, V.V., Kondakova, T.N., 2003. Degradation of performance of the navigation GPS system in geomagnetically disturbed conditions. GPS Solutions 7, No. 2; LINKSpringer: DOI 10.1007/s10291-003-0053-7.

Al'perovich, L.S., Fedorov, E.N., Volgin, A.V., 1991. Doppler sounding a tool for the study of the MHD wave structure in the magnetosphere. Journal of Atmospheric and Solar-Terrestrial Physics 53, 581–586.

Baker, D.M., Davies, K., 1969. F2-region acoustic waves from severe weather. Journal of Atmospheric and Solar-Terrestrial Physics 31, 1345–1352.

Bertin, F., Testud, J., Kersley, L., 1975. Medium scale gravity waves in the ionospheric F-region and their possible origin in weather disturbances. Planet Space Science 23, 493–507.

Bertin, F., Testud, J., Kersley, L., Rees, P.R., 1978. The meteorological jet stream as a source of medium scale gravity waves in the thermosphere: an experimental study. Journal of Atmospheric and Solar-Terrestrial Physics 40, 1161–1183.

Coster, A.J., Foster, J.C., Erickson, P.J., Rich, F.J., 2001. Regional GPS mapping of storm enhanced density during the July 15–16 2000 geomagnetic storm. Proceedings of International Beacon Satellite Symposium, June 4–6, 2001, Boston College, Institute for Scientific Research, Chestnut Hill, MA, USA, pp. 176–180.

Davies, K., 1969. Ionospheric Radio Waves. Blaisdell Publishing Company, A Division of Ginn and Company, Waltham, Massachusetts, Toronto, London.

Davies, K., Hartmann, G.K., 1976. Short-period fluctuations in total columnar electron content. Journal of Geophysical Research 81, 3431–3434.

Davies, K., Jones, J.E., 1971. Three-dimensional observations of traveling ionospheric disturbances. Journal of Atmospheric and Solar-Terrestrial Physics 33 (1), 39–46.

Duffus, H.J., Boyd, G.M., 1968. The association between ULF geomagnetic fluctuations and Doppler ionospheric observations. Journal of Atmospheric and Solar-Terrestrial Physics 30, 481–495.

Francis, S.H., 1974. A theory of medium-scale traveling ionospheric disturbances. Journal of Geophysical Research 79, 5245–5259.

Gurtner, W., 1993. RINEX: The Receiver Independent Exchange Format Version 2. http://igscb.jpl.nasa.gov:80/igscb/data/format/rinex2.txt

Hines, C.O., 1960. Internal atmospheric gravity waves at ionospheric heights. Canadian Journal of Physics 38 (8), 1441–1481.

Hines, C.O., Reddy, C.A., 1967. On the propagation of atmospheric gravity waves through regions of wind shear. Journal of Geophysical Research 72 (5), 1015–1034.

Hocke, K., Schlegel, K., 1996. A review of atmospheric gravity waves and traveling ionospheric disturbances: 1982–1995. Annales Geophysicae 14 (5), 917–940.

Hofmann-Wellenhof, B., Lichtenegger, H., Collins, J., 1992. Global Positioning System: Theory and Practice. Springer, Wien, New York, 327pp.

Huang, Yinn-Nien., Cheng, Kang., Sen-Wen, Chen., 1985. On the detection of acoustic-gravity waves generated by typhon by use of real time HF Doppler frequency shift sounding system. Radio Science 20(4), 897–906.

Hung, R.G., Phan, T., Smith, R.E., 1978. Observation of gravity waves during the extreme tornado outbreak of 3 April 1974. Journal of Atmospheric and Solar-Terrestrial Physics 40, 831–843.

Jacobson, A.R., Carlos, R.C., 1991. A study of apparent ionospheric motions associated with multiple travelling ionospheric disturbances. Journal of Atmospheric and Solar-Terrestrial Physics 53 (1/2), 53–62.

Jacobson, A.R., Carlos, R.C., Massey, R.S., Wu, G., 1995. Observations of traveling ionospheric disturbances with a satellite-beacon radio interferometer: seasonal and local time behavior. Journal of Geophysical Research 100, 1653–1665.

Kalikhman, A.D., 1980. Medium-scale traveling ionospheric disturbances and thermospheric winds in the F-region. Journal of Atmospheric and Solar-Terrestrial Physics 42 (8), 697–703.

Kersly, L., Rees, P.R., 1982. Tropospheric gravity waves and their possible association with medium-scale travelling ionospheric disturbances. Journal of Atmospheric and Solar-Terrestrial Physics 44 (2), 147–159.

Klobuchar, J.A., 1986. Ionospheric time-delay algorithm for single-frequency GPS users. IEEE Transactions on Aerospace and Electronics System 23 (3), 325–331.

Klostermeyer, J., Rottger, J., 1976. Simultaneous geomagnetic and ionospheric oscillations caused by hydromagnetic waves. Planetary Space Science 24, 1065–1071.

Mannucci, A.J., Ho, C.M., Lindqwister, U.J., et al., 1998. A global mapping technique for GPS-drived ionospheric TEC measurements. Radio Science 33, 565–582.

Mercier, C., 1986. Observations of atmospheric gravity waves by radiointerferometry. Journal of Atmospheric and Solar-Terrestrial Physics 48, 605–624.

Mercier, C., 1996. Some characteristics of atmospheric gravity waves observed by radio-interferometry. Annales Geophysics 14, 42–58.

Okuzawa, T., Davies, K., 1981. Pulsations in total electron content. Journal of Geophysical Research 86, 1355–1363.

Oliver, W.L., Otsuka, Y., Sato, M., Takami, T., Fukao, S., 1997. A climatology of F region gravity waves propagation over the middle and upper atmosphere radar. Journal of Geophysical Research 102, 14449–14512.

Otsuka, Y., Ogawa, T., Saito, A., Tsugawa, T., Fukao, S., Miyazaki, S., 2002. A new technique for mapping of total electron content using GPS network in Japan. Earth, Planets and Space 54 (1), 63–70.

Potapov, A.S., Polyushkina, T.N., Afraimovich, E.L., Lipko, Y.V., 2002. Transequatorial propagation of the Pc1 emission on 23 October 1997. Journal of Geophysical Research 107(A7), 10.1029/2001JA000225.

Rishbeth, H., Garriot, O.K., 1964. Relationship between simultaneous geomagnetic and ionospheric oscillations. Radio Science 68D, 339–343.

Saito, A.M., Nishimura, M., Yamamoto, M., Fukao, S., Kubota, M., Shiokawa, K., Otsuka, Y., Tsugawa, T., Ogawa, T., Ishii, M., Sakanoi, T., Miyazaki, S., 2001. Traveling ionospheric disturbances detected in the FRONT campaign. Geophysical Research Letters 28, 689–692.

Saito, A., Nishimura, M., Yamamoto, M., Fukao, S., Tsugawa, T., Otsuka, Y., Miyazaki, S., Kelley, M.C., 2002. Observations of traveling ionospheric disturbances and 3-m scale irregularities in the nighttime F-region ionosphere with the MU radar and a GPS network. Earth, Planets and Space 54 (1), 31–44.

Shan, S.J., Lin, J.Y., Kuo, F.S., et al., 2002. GPS phase fluctuation observed along the American sector during low irregularity activity months of 1997–2000. Earth, Planets and Space 54 (2), 141–152.

Shiokawa, K., Otsuka, Y., Ejiri, M.K., Sahai, Y., Kadota, T., Ihara, C., Ogawa, T., Igarashi, K., Miyazaki, S., Saito, A., 2002. Imaging observations of the equatorward limit of midlatitude traveling ionospheric disturbances. Earth, Planets and Space 54 (1), 57–62.

Skone, S., de Jong, M., 2000. The impact of geomagnetic substorms on GPS receiver performance. Earth, Planets and Space 52, 1067–1071.

Skone, S., de Jong, M., 2001. Limitations in GPS receiver tracking performance under ionospheric scintillation. Physics and Chemistry of the Earth, Part A 26 (6–8), 613–621.

Somsikov, V.M., 1995. On the mechanism of formation of atmospheric inhomogeneities in the solar terminator region. Journal of Atmospheric and Terrestrial Physics 57, 75–83.

Spoelstra, T.A.Th., 1992. Combining TIDs observations: NNSS and radio interferometry data. Journal of Atmospheric and Solar-Terrestrial Physics 54, 1185–1195.

Stobie, J.G., Einaudi, F., Uccellini, L.W., 1983. A case study of gravity waves-convective storms interaction: 9 May 1979. Journal of the Atmospheric Science 40 (12), 2804–2830.

Velthoven, P.F.J., Mercier, C., Kelder, H., 1990. Simultaneous observations of travelling ionospheric disturbances by two-dimensional radio interferometry and the differential Doppler technique applied to satellite signals. Journal of Atmospheric and Solar-Terrestrial Physics 52 (4), 305–312.

Waldock, J.A., Jones, T.B., 1984. The effects of neutral winds on the propagation of medium-scale atmospheric gravity waves at mid-latitudes. Journal of Atmospheric and Solar-Terrestrial Physics 46, 217–231.

Waldock, J.A., Jones, T.B., 1986. HF Doppler observations of medium-scale traveling ionospheric disturbances at mid-latitudes. Journal of Atmospheric and Solar-Terrestrial Physics 48, 245–260.

Waldock, J.A., Jones, T.B., 1987. Source regions of medium-scale travelling ionospheric disturbances observed at mid-latitudes. Journal of Atmospheric and Solar-Terrestrial Physics 49 (2), 105–114.

Yakovets, A.F., Kaliev, M.Z., Vodyannikov, V.V., 1999. An experimental study of wave packets in travelling ionospheric disturbances. Journal of Atmospheric and Solar-Terrestrial Physics 45 (8), 629–639.